Measurement of 2s and 3s electron-spin densities in iron metal and Fe_2O_3 †

Cheng-jyi Song*, Jan Trooster‡, and N. Benczer-Koller
Physics Department, Rutgers University, New Brunswick, New Jersey 08903
(Received 19 November 1973)

The 2s and 3s electron-spin densities at the nuclear site of the ^{57}Fe nucleus in iron metal and Fe_2O_3 were measured by a new technique combining the Mössbauer effect with electron spectroscopy. The ratios of wave functions at the nucleus $|\Psi^{\uparrow}_{ns}(0)|^2 / |\Psi^{\downarrow}_{ns}(0)|^2$ for 2s and 3s electrons were measured for iron metal and Fe_2O_3, and were found to agree in sign and order of magnitude with theoretical calculations of the core-polarization contributions to the magnetic hyperfine interactions.

I. INTRODUCTION

The total hyperfine field at ^{57}Fe nuclei embedded in magnetic lattices has been measured by a variety of techniques. It is now established that the main contributions to the hyperfine field arise from polarization of core electrons by the 3d electrons. A new technique which combines Mössbauer and internal-conversion spectroscopy has been developed to determine the net spin polarization at the nuclear site of s electrons from each individual subshell. The method has been applied to iron metal[1] and Fe_2O_3. The details of the experiment and the analysis of the data are presented below. The results obtained for the spin polarization of 2s and 3s electrons in Fe metal and Fe_2O_3 will be compared with theoretical predictions.

II. ORIGIN OF MAGNETIC HYPERFINE FIELDS

In 1960, the Zeeman effect was observed for the first time in a nuclear transition. The high resolution of Mössbauer recoilless processes made it possible to resolve the six components of the γ transition between the $3/2^-$ first excited state and the $1/2^-$ ground state of the ^{57}Fe nucleus embedded in an iron matrix. The magnetic degeneracy of the states is lifted by the hyperfine interaction between the nucleus and surrounding electrons.

Fermi and Fermi and Segrè[2] showed that the Hamiltonian for the interaction between a single electron and a nucleus can be written as

$$\mathcal{H} = -gg_I\mu_B\mu_N\{(8\pi/3)\delta(\vec{r})\vec{I}\cdot\vec{s} + r^{-3}\vec{I}\cdot\vec{l} + [3r^{-5}(\vec{I}\cdot\vec{r})(\vec{s}\cdot\vec{r}) - r^{-3}\vec{I}\cdot\vec{s}]\}, \quad (1)$$

where $\vec{l}$, $\vec{s}$, and $\vec{I}$ represent, respectively, the electron orbital, electron spin, and nuclear spin angular momentum operators; g and g_I are the electronic and nuclear g factors; and μ_B and μ_N are the Bohr and nuclear magnetons.

The $\vec{I}\cdot\vec{l}$ term in Eq. (1) arises from the dipolar interaction of the nuclear spin with the electron orbital angular momentum. The $\vec{I}\cdot\vec{s}$ term describes the dipolar interaction between electronic and nuclear magnetic moments. The dipolar terms vanish for S state ions and for ions in cubic symmetry. The δ function term, which is called the Fermi contact term, arises from the electron spin magnetization inside the nucleus and is nonzero only for s electrons.

The contact term $\mathcal{H}_c$ can be expressed in terms of an effective field at the nucleus $\vec{H}_e$; $\mathcal{H}_c = -g_I\mu_N\vec{H}_e\cdot\vec{I}$, where $\vec{H}_e = (8\pi/3)g\mu_B\vec{S}|\psi(0)|^2$, $|\psi(0)|^2$ is the s electron's density at the nucleus, and $\vec{S}$ is the total electronic spin in the s shell in question.

Historically, the contact term was first considered for systems with unpaired s electrons. Fermi and Segrè[2] first estimated the effect of exchange in producing a contact term in the closed $(6s)^2$ shell of Tl. No hyperfine fields are expected in closed shell systems with paired s electrons, or in half-filled S state ions such as Fe^{3+} or Mn^{2+} in the $3d^5\ ^6S$ state. The existence of large magnetic hyperfine fields in these ions led Abragam and Pryce[3] to consider admixtures of configurations in which 1s, 2s, or 3s electrons were promoted to a higher s state. Their calculations yielded hyperfine interactions of the right sign, but ten times smaller than the observed value. Sternheimer[4] then suggested that a polarization of all the core electrons (1s, 2s, and 3s) by the net spin of the 3d electrons would produce a large nonzero spin density at the nucleus and hence a large hyperfine field. The importance of the core electron contribution to $\vec{H}_e$ was realized when the large hyperfine field in iron was found to be negative,[5] that is, opposite to the direction of the magnetization of the 3d electrons. No other contribution could be found to produce such a large negative field.

A simplified picture of the mechanism of "core-polarization" is given in Fig. 1. The exchange interaction between the 3d electrons and the core s electrons causes a repulsion of electrons with antiparallel spin and an effective attraction between parallel spin electrons, resulting in different radial wave functions for electrons of opposite sign and a net spin density at the nucleus. A magnetic hyperfine field at the nucleus results which is propor-

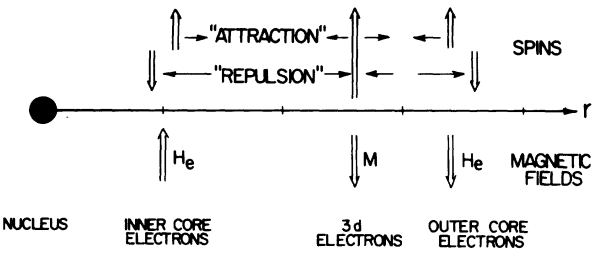

FIG. 1. Schematic representation of spins and average position of inner core, outer core, and 3d electrons, local magnetic hyperfine fields and exchange interactions in an iron ion.

tional to the total spin of the d shell and is given by

$$\vec{H}_e = (8\pi/3) g\mu_B \vec{S} \sum_{ns} [\,|\psi^{\uparrow}_{ns}(0)|^2 - |\psi^{\downarrow}_{ns}(0)|^2], \qquad (2)$$

where $|\psi^{\uparrow}_{ns}(0)|^2 - |\psi^{\downarrow}_{ns}(0)|^2$ is the net spin density in the ns shell for $S=1$, and n runs over all s shells to be considered. "Inner" shell electrons exhibit a negative spin density at the nucleus, which in turn produces a negative hyperfine field, while the opposite is true of "outer" shell electrons.

Watson and Freeman[6] have applied the spin or exchange polarized Hartree-Fock method to investigate the contribution of paired electrons to $\vec{H}_e$ in the case of transition metal ions. Detailed results were obtained for Mn^{2+} which is isoelectronic with Fe^{3+}. Bagus and Liu[7] calculated the individual ns shell contributions to $\vec{H}_e$ for atomic Fe. Their results, which are very similar to those obtained by Watson and Freeman for Mn^{2+}, are given in Table I. The dominant contribution to H_e is seen to arise from the polarization of the $2s$ shell. The net spin density in this shell is antiparallel to the $3d$ electron spin and the resulting field at the nucleus is therefore negative.

The total hyperfine field has been measured by a variety of techniques such as ESR, NMR, or Mössbauer spectroscopy. These experiments, however, cannot distinguish the core contribution from those of other hyperfine interactions, such as the dipolar field of neighboring atoms and contributions from unquenched angular momentum. Moreover, $\vec{H}_e$ is a sum of contributions of opposite sign, each of which corresponds in turn to a small difference between large numbers. The present experiment is aimed at determining separately the *individual* s shell contributions to $\vec{H}_e$ as a further test of the theoretical model and calculations.

III. MEASUREMENT OF MICROSCOPIC CONTRIBUTIONS TO HYPERFINE FIELDS

A nucleus in a low lying excited state may decay to the ground state by emission of γ rays or internal conversion electrons. The probability for internal conversion α is defined as the ratio of internal conversion electrons to the γ ray yield. The conversion probability is proportional to the electronic charge density; in particular, as will be shown below, for magnetic dipole transitions $\alpha(M1)$ is proportional to the electronic charge density at the nucleus. Since only s electrons have an appreciable charge density over the nuclear region, $M1$ conversion proceeds mainly by emission of s electrons, and thus is a particularly selective process. Given the difference in electron radial wave functions produced by the core polarization mechanism, one would then expect that the yield of internally converted ns electrons would differ for electrons with opposite spin within a particular ns shell.

Consider the $M1$ decay from the 14.4 keV, $I=3/2^-$, first excited state of ^{57}Fe to the $I=1/2^-$ ground state. This transition proceeds mostly through internal conversion with a total internal conversion coefficient $\alpha = 8.26 \pm 0.19$.[8] Figure 2 displays the nuclear level scheme and two of the six allowed nuclear transitions; the $\Delta m_I = 1$ ($m_{Ii} = -\frac{3}{2} \rightarrow m_{If} = -\frac{1}{2}$) and $\Delta m_I = -1$ ($m_{Ii} = \frac{3}{2} \rightarrow m_{If} = \frac{1}{2}$) decays correspond to total angular momentum changes of the emitted internal conversion ns electrons $\Delta m_e = -1$ ($m_{ei} = \frac{1}{2}$), and $\Delta m_e = 1$ ($m_{ei} = -\frac{1}{2}$), respectively. The direction of the $3d$ electron magnetization was chosen as the quantization axis.

For an $M1$ internal conversion transition in the $K(1s)$, $L_I(2s)$, $M_I(3s)$, or $N_I(4s)$ shells, the initial electron is in an $s_{1/2}$ state; the addition of one unit of angular momentum with no parity change leads to either $s_{1/2}$ or $d_{3/2}$ final continuum states. Conversion into a $d_{3/2}$ state is more than ten times weaker than conversion into a final s state[9] and was ignored in the following discussion and analysis.

TABLE I. Column 2 displays the individual s-electron density at the nuclear site $|\psi_{ns}(0)|^2$ for each individual s subshell for Mn^{++}; column 3 gives the relative spin density $\delta_{ns} = [\,|\psi^{\uparrow}_{ns}(0)|^2 / |\psi^{\downarrow}_{ns}(0)|^2] - 1$; Columns 4 and 5 indicate the individual and the net contributions to the magnetic field H_e at the nucleus. ↑ (↓) denotes electrons with spin parallel (antiparallel) to the $3d$-shell net spin. These data were obtained from the calculation of Bagus and Liu (Ref. 7).

	$\lvert\psi_{ns(0)}\rvert^2$	$\frac{\lvert\psi^{\uparrow}_{ns(0)}\rvert^2}{\lvert\psi^{\downarrow}_{ns(0)}\rvert^2} - 1$	H_{ns} (kG)	$H^{\uparrow}_{ns} + H^{\downarrow}_{ns}$ (kG)
$1s\uparrow$	5386.490	-8.7×10^{-6}	2849698	
$1s\downarrow$	5386.537		−2849723	−25
$2s\uparrow$	493.668	−0.00514	261173	−1346
$2s\downarrow$	496.213		−262519	
$3s\uparrow$	68.587	+0.0210	36286	+754
$3s\downarrow$	67.162		−35532	
$4s\uparrow$	3.600	+0.29	1905	+488
$4s\downarrow$	2.679		−1417	

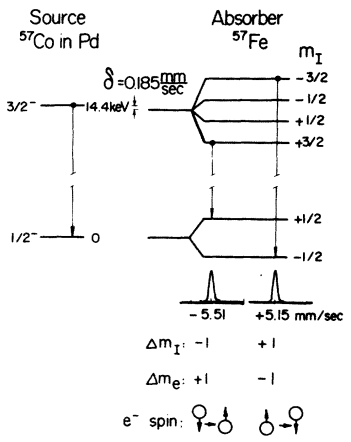

FIG. 2. Energy-level diagram of ^{57}Fe indicating the $\Delta m_I = \pm 1$ transitions and the corresponding changes in angular momentum of the internally converted electrons.

The angular distribution functions $F_L^M(\theta)$ of the converted ns electrons from an $M1$ nuclear transition for either $L = M = 1$ or $L = -M = 1$, were calculated by Rose *et al.*[10] and are given by

$$F_1^1(\theta) = 8\left|R_{-1,\downarrow}\right|^2, \tag{3a}$$

$$F_1^{-1}(\theta) = 8\left|R_{-1,\uparrow}\right|^2, \tag{3b}$$

and

$$R_{-1,\tau} = \int_0^\infty r^2\, dr h_1^{(1)}(kr)(f_{-1}g_\tau + g_{-1}f_\tau), \tag{4}$$

where $\tau = +\frac{1}{2}(\uparrow)$ or $-\frac{1}{2}(\downarrow)$ is the spin of the initial bound electrons, f_τ and g_τ are the small and large components of the radial wave function of the bound electron, f_{-1} and g_{-1} are the wave functions for the free electron; final $d_{3/2}$ states are neglected.

Equation (3a) corresponds to an $L = M = 1$ nuclear transition and pertains to conversion of electrons with initial spin down with respect to the quantization axis. Similarly, Eq. (3b) represents the $L = -M = 1$ nuclear transition and only electrons with initial spin up are converted. The spherical Hankel function $h_1^{(1)}(kr)$ behaves like a δ function; thus one might expect that the main contribution to the electron yield comes mostly from the electron density in the nuclear region. In fact, Band *et al.*,[11] Anderson *et al.*,[12] and Fujioka[13] have examined in detail the region of the atom where the conversion process occurs. They have concluded that for $M1$ s electron emission, conversion is produced in a region well within the first node of the radial wave functions of both the orbital and free electrons. These effects result in a definite relation between the value of the electronic wave function at the nucleus and its behavior throughout the region of conversion formation, and further leads to a direct proportionality between the radial integrals and the electronic density at the nucleus:

$$\alpha^\tau \simeq \left|R_{-1,\tau}^{ns}\right|^2 \simeq \left|\psi_{ns}^\tau(0)\right|^2, \tag{5}$$

where the nonrelativistic wave function $\psi_{ns}^\tau(0)$ replaces the relativistic wave functions of Eq. (4) in the nonrelativistic limit.

The comparison of Eq. (5) with Eq. (2) shows that the contribution to the magnetic hyperfine interaction has the same dependence on the radial wave function of the orbital ns electron as the internal conversion coefficient of the corresponding ns electron. Accordingly, $\alpha\uparrow$ differs from $\alpha\downarrow$ and the ratio $\alpha\uparrow/\alpha\downarrow$ is directly proportional to the ratio of intensities of conversion electrons emitted in the decays $\Delta m_I = +1$ and $\Delta m_I = -1$, respectively. Hence $(\alpha\uparrow/\alpha\downarrow - 1)$ becomes a measure of the net electronic polarization at the nuclear site.

In the above discussion no mention was made of the final state of the atom.[14] For example, the initial state of the Fe^{3+} ion is $(3d)^5\,{}^6S$. When a spin up electron is ejected the atom is left in a final ^5S state, while when a spin-down electron is emitted, the final state is ^7S. This distinction is of note when the energy of the ejected electron is measured,[15] and it is the cause for the multiplet structure and intensity seen in photoemission experiments. In the present experiment transitions with predetermined Δm_e are selected and the ratio of intensities of the two lines is governed only by the Clebsch-Gordan coefficients. Thus, the transition $m_{ei} = -\frac{1}{2} \rightarrow m_{ef} = +\frac{1}{2}$ leading to a final atomic state of spin $S_f = 3$, $M_f = 3$ proceeds with probability 1 times the matrix element of the transition, while the transition $m_{ei} = +\frac{1}{2} \rightarrow m_{ef} = -\frac{1}{2}$ can leave the final atom in states of spin $S_f = 2$ or 3 and $M_f = 2$ with corresponding probability $\sqrt{\frac{5}{6}}$ and $\sqrt{\frac{1}{6}}$, respectively, times the same matrix element. When these are added incoherently it is obvious that the relative intensities expected for the two transitions differ only through the appearance in the matrix elements of different radial wave functions for the bound electron. Similar considerations apply when other possible configurations contributing to the final ^5S state are considered.[14]

IV. EXPERIMENT

The main feature of the experiment involves the selective excitation of either the $m_I = +\frac{3}{2}$ or the $m_I = -\frac{3}{2}$ substates of ^{57}Fe nuclei by absorption of 14.4 γ rays emitted from an unsplit ^{57}Co(Pd) source moved at the constant velocities corresponding to recoilless absorption into the proper substates. The subsequently emitted 1s (6.3 keV), 2s (13.6 keV), or 3s (14.3 keV) internal conversion electrons were selected by an electron spectrometer. The details of the experimental apparatus are described below.

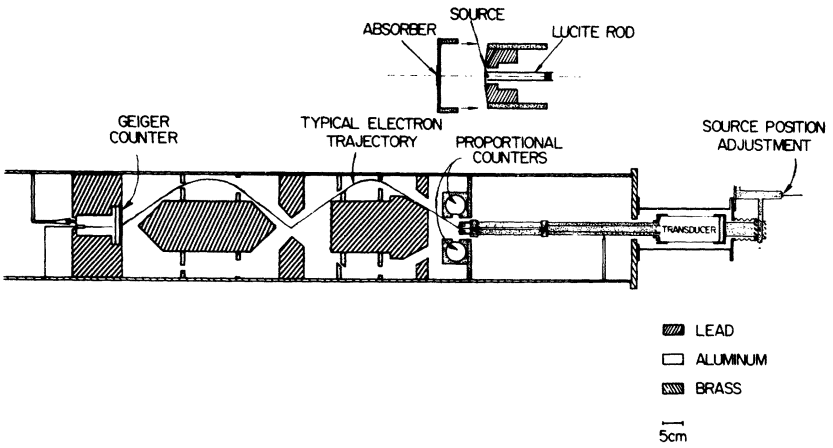

FIG. 3. Diagram of the magnetic solenoid electron spectrometer incorporating the Mössbauer velocity drive.

A. Electron spectrometer

The electron spectrometer used in this experiment was built in 1941[16] (Fig. 3). It is an iron-free magnetic solenoid, 170 cm in length with a diameter of 25 cm. The electron trajectory is defined by a two cycle aluminum-lined lead baffle. Adjustable slits on the outer rim of the baffle fixed the entrance angle of the transmitted electrons at 45° The exit slit width was adjusted for maximum transmission (~1%) at an intrinsic resolution of 2%. The β spectrometer was energized by a current regulated power supply, which could deliver up to 100 A with a regulation better than 0.05%. The current could be controlled by an external reference voltage, which allowed automatic sweep of the current with synchronous display of the electron spectrum in a multichannel analyzer.

An end-window Geiger-Müller counter was used as the electron detector. The counter window was made of Formvar, 25 $\mu g/cm^2$ thick supported by a copper mesh; the counter was filled with ethyl alcohol vapor to a pressure of 17 Torr.

B. Velocity drive

A Mössbauer velocity transducer of the type described by Kankeleit[17] was mounted outside the solenoid. The Mössbauer source was glued to an extension rod running through the tube bearing the absorber and supported by two circular leaf springs. The transducer and its extension were supported at two points: inside the β spectrometer the extension tube rested on a V-type support; outside the β spectrometer the transducer was fixed to the end plate through bellows, thus allowing the position of the absorber to be externally adjusted in three mutually perpendicular directions for optimum transmission and resolution (Fig. 3).

C. Velocity regulation

A conventional feedback system with operational amplifiers was used to regulate the velocity. As explained in Sec. III the source was moved at two velocities corresponding to excitation of absorber nuclei into the $m_I = +\frac{3}{2}$ and $-\frac{3}{2}$ states, respectively, while the yield of internal conversion electrons emitted in the decay of these states was measured. In order to measure alternately the resonant and background radiation modes the periodic velocity shown in Fig. 4 was adopted. Synthetization of the reference wave form used is schematically indicated in Fig. 5. Because of the isomer shift between source and absorber, the absolute values of the on-resonance velocities differ by 0.37 mm/sec for iron metal and by 0.13 mm/sec for the oxide sample. To compensate for this difference the ampli-

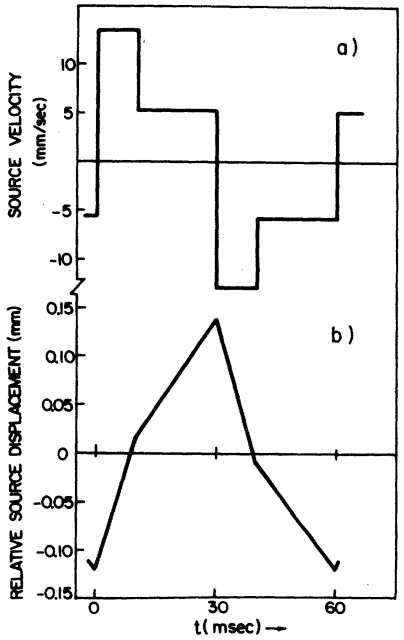

FIG. 4. (a) Periodic velocity reference wave form and (b) corresponding displacement of the source relative to the absorber.

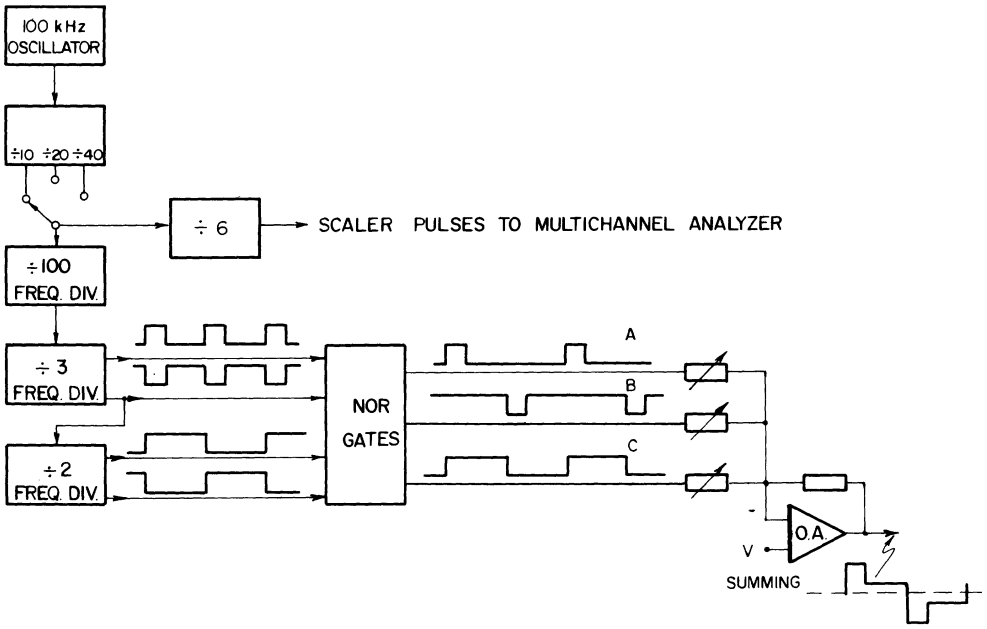

FIG. 5. Reference voltage synthesis.

tudes of the off-resonant velocities were adjusted independently, so that the total distance traveled by the source in each half-period was the same. Period lengths of 60 msec and 120 msec were used. During a measurement, the number of detected electrons was stored in 100 channels of a multichannel analyzer, operated in the multiscale mode in synchronization with the periodic motion. For exploratory measurements the Mössbauer transducer could be operated in the constant acceleration mode corresponding to a symmetric triangular reference voltage.

D. X-ray detectors

γ and x radiations scattered from the absorber were monitored by two proportional counters mounted inside the β spectrometer (Fig. 3). They were installed opposite each other, 4 cm away from the absorber. The edge of the circular 1-in. -diam windows were level with the plane of the absorber. The pulses of each counter were separately amplified and analyzed in single channel analyzers. Initially these counters were used to monitor the rate of K-electron conversion through detection of the 6.3-keV K x rays that accompany K conversion. Ultimately, they were used to determine the exact positions of the source as a function of time, as described in Sec. V.

E. Sources and absorbers

Several 50-mCi ^{57}Co(Pd) Mössbauer sources with an active area of 2 mm diameter were used for about two half-lives each. Absorbers were prepared by evaporating 92% enriched ^{57}Fe to a thickness of 35 μg/cm^2 and 1 cm diameter on a lead-free microscope coverglass 0.1 mm thick. The Mössbauer absorption spectrum of such an evaporated layer showed broad lines as well as a paramagnetic component. After annealing for 3 h at 450 °C in a hydrogen atmosphere, the linewidth was reduced to 0.27 mm/sec and the paramagnetic component disappeared. Fe_2O_3 absorbers were made by oxidizing a similarly evaporated iron foil in the oxygen atmosphere at 450 °C.

The supporting glass plate was taped on the end of an aluminum extension tube which was fixed to the Mössbauer velocity transducer. The glass backing of the absorber foil served as an efficient stopper for electrons emitted by the Mössbauer source. The details of the Mössbauer source-absorber geometry are shown in the insert in Fig. 3. A 1.3-mm-thick, 2-mm-diam lead collimator limited the active area of the absorber to the maximum compatible with the required spectrometer resolution. The source-absorber distance d was adjustable. Most experiments were carried out for $d = 2.75$ and 4 mm. Typical counting rates at $d = 2.75$ mm are listed in Table II.

F. Electron spectra

Figures 6(a) and 6(b) show electron spectra obtained with the Mössbauer source moving at resonant (open circles) or off-resonant (solid circles) velocities as a function of electron momentum. Figures 6(c) and 6(d) show the internal conversion K, L and M lines of ^{57}Fe after subtraction of the

TABLE II. Typical counting rates of internal-conversion electrons at a source-absorber distance of 2.75 mm. The K-line counting rate is very sensitive to the thickness of the Geiger-Müller counter window and varied widely for different windows. The cosmic-ray background was of the order of 26 counts/min.

electron shell \ Yield (counts/min) (50 mCi source)	Average yield at resonance $\langle Y^{\pm}\rangle$	Average yield off resonance $\langle B^{\pm}\rangle$	$\frac{\langle Y^{\pm}\rangle - \langle B^{\pm}\rangle}{\langle B^{\pm}\rangle}$
K	2000	500	3.0
L	1500	620	1.4
$M+N$	520	380	0.37

nonresonant background. The nonresonant background consists of two contributions: a line spectrum of external conversion photoelectrons ejected by the 14.4-keV γ rays and a continuous spectrum of tails of lines corresponding to external conversion of higher-energy γ rays superposed on the energy-independent room (cosmic rays) background.

G. Mössbauer spectra

Absorption Mössbauer spectra were run on all absorbers prior to mounting in the β spectrometer. These spectra indicated that the Fe absorbers were polarized in the plane of the absorber while the Fe_2O_3 absorbers remain unpolarized because of the large crystalline magnetic anisotropy in Fe_2O_3. Furthermore, the spectra showed that the main constituent of the oxide absorbers was $\alpha-Fe_2O_3$, with a small amount of $\gamma-Fe_2O_3$.

A typical Mössbauer spectrum measured on the L internal conversion electrons of the ^{57}Fe absorber is shown in Fig. 7(a). This spectrum was obtained with the Mössbauer spectrometer operated in the constant acceleration mode and with a source-absorber separation of 2 mm. Also shown on Fig. 7(b) is the spectrum of scattered 6.3-keV K x rays, which was obtained simultaneously with that of Fig. 7(a). The line shapes are distorted because the source-absorber distance was comparable to their diameters.

H. Accuracy and reproducibility

The stability of the velocity drive was mainly governed by the stability of the reference wave and by the sensitivity of the transducer. Referring to Fig. 5, the amplitudes of signals A and C were determined by temperature compensated Zener diodes (type PS 3536), which had a temperature coefficient of 0.005%/°C. Signal B is the output of a NOR-gate whose temperature coefficient is estimated to be less than 0.1%/°C. Variation in amplitude of B affects the isomer shift compensation. For the actual measurements the amplitudes of B and C were chosen, such that the effect of amplitude variations on the intensity ratio measured was minimal. A change in on-resonance velocity amplitude of 0.1% caused a change in the background corrected intensity ratio of (0.01–0.02)%. Due to the finite gain in the velocity feedback, the velocity is not constant but changes linearly with time by about 4%. This variation was determined by measuring the electron intensity as function of time within a

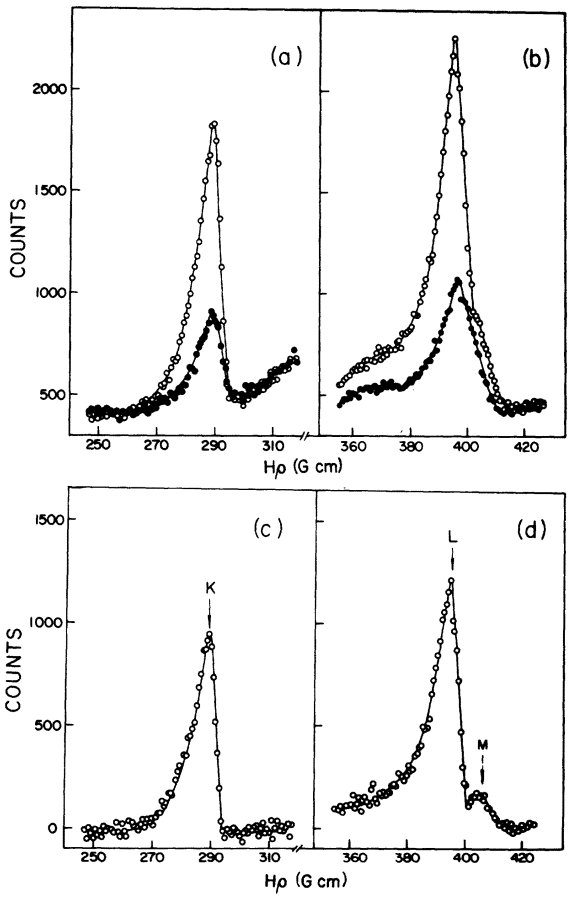

FIG. 6. Electron spectra from $^{57}Fe_2O_3$ absorber (a) at the K line field (the open circles correspond to the resonant velocity and the solid circles to the off-resonant velocity (b) at the L and M lines field; (c) net internal conversion K line, and (d) net internal conversion L and M lines.

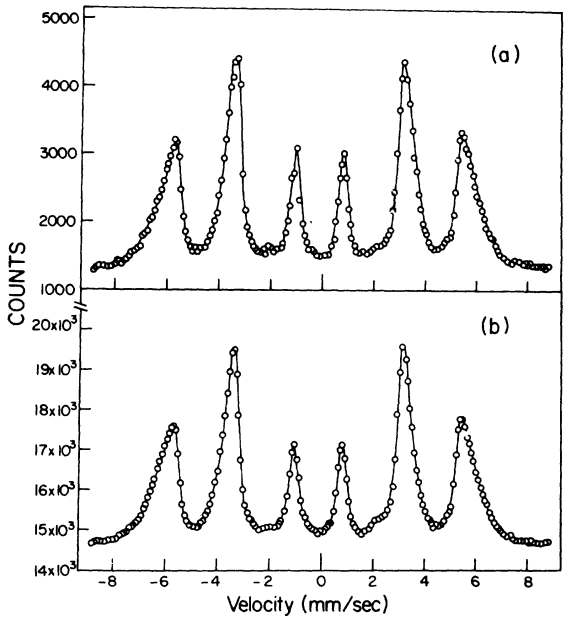

FIG. 7. Mössbauer spectra of (a) internal conversion L electrons and (b) scattered 6.3-keV K x rays.

period. The velocity amplitude was set to correspond with a position on the outer slope of the resonance line and the velocity change was derived by correlating the measured change in intensity with the line shape observed in the constant acceleration mode. Thus, during an actual measurement a small part of the Mössbauer line around the nearly flat peak maximum was scanned. In addition, a damped ringing in phase with the periodic motion occurred after each velocity jump. The measurements were begun after this ringing was damped to less than 1%.

The transducer stability is sensitive to both temperature changes and the stray field of the β spectrometer. As the transducer was inside the vacuum chamber, its temperature was that of the water-cooled spectrometer and thus stable to within a degree. Hence, the effect of the temperature variations on the sensitivity was neglected. The effect of the stray field on the sensitivity of the transducer could be very accurately measured by observing the intensity ratios of the $\Delta m = \pm 1$ lines without isomer shift compensation. Under these circumstances, the electron yield was measured for some particular drive velocity on the inner and outer slope of the resonance lines, rather than on the relatively flat peaks; thus the measured ratio becomes a very sensitive function of the velocity. Using this method, and amplitude difference of 0.13% was measured for β spectrometer fields corresponding to K and L electron detection. As this accuracy is approximately equal to the reproducibility of the velocity setting no attempt was made to correct for this deviation. It is estimated that this change in velocity amplitude results in a change in yield of at most 0.02%.

V. MEASUREMENTS, ANALYSIS, AND TESTS

The total yield Y of electrons counted by the detector can be divided into three parts: $Y = I + E + C$.

(a) The intensity I of internal conversion electrons is a complicated function of the source-absorber distance due to both the change in solid angle and the cosine spread in velocities "seen" by the absorber.

(b) The background E of electrons ejected from the absorber by other processes (mainly photoelectrons) is independent of the velocity of the Mössbauer source, but does depend on the source-absorber distance.

(c) The constant background C due to external sources amounted to only a small fraction of the total intensity.

To extract the true ratio of internal conversion from the $m_I = \pm\frac{3}{2}$ levels from the raw data, it was necessary to (a) subtract from the measured intensities Y, the background of $B = C + E$ corresponding to the same source position as prevailed for the measurement of Y and (b) correct the intensity ratio $R = (Y^+ - B^+)/(Y^- - B^-) = I^+/I^-$ for the solid angle effects which arise because the source is on the average closer to the absorber during the portion of the cycle corresponding to the decay of the $m_I = -\frac{3}{2}$ state than during the period corresponding to the decay of the $m_I = +\frac{3}{2}$ state [Fig. 8(c)]. To apply both of these corrections, the position of the source as a function of time had to be accurately known. To this end, the intensity of nonresonantly scattered x and γ radiation with energy higher than 14.4 keV was measured with the two proportional counters located above and below the absorber and stored in a second multichannel analyzer run synchronously with the analyzer recording the electron intensity. Data collection and reduction are probably best discussed with the help of Fig. 8 which represents the results of a measurement. In this particular case, the β spectrometer was set for detection of K electrons. The amplitude of the off- and on-resonance velocities was adjusted in the manner previously described. In spite of the obvious nonlinear dependence of the γ-ray intensity on the displacement, it was possible to determine from Fig. 8(d) which "off-resonance" and "on-resonance" channels correspond to the *same* source-absorber separation. The contents of the off-resonance channels [Fig. 8(c)] were then subtracted from those of the corresponding on-resonance channels. Finally the solid angle effect was determined from measured I^+/I^- ratios for the L and M electrons by normalizing these ratios by $R_K = (I^+/I^-)_K$. Since all

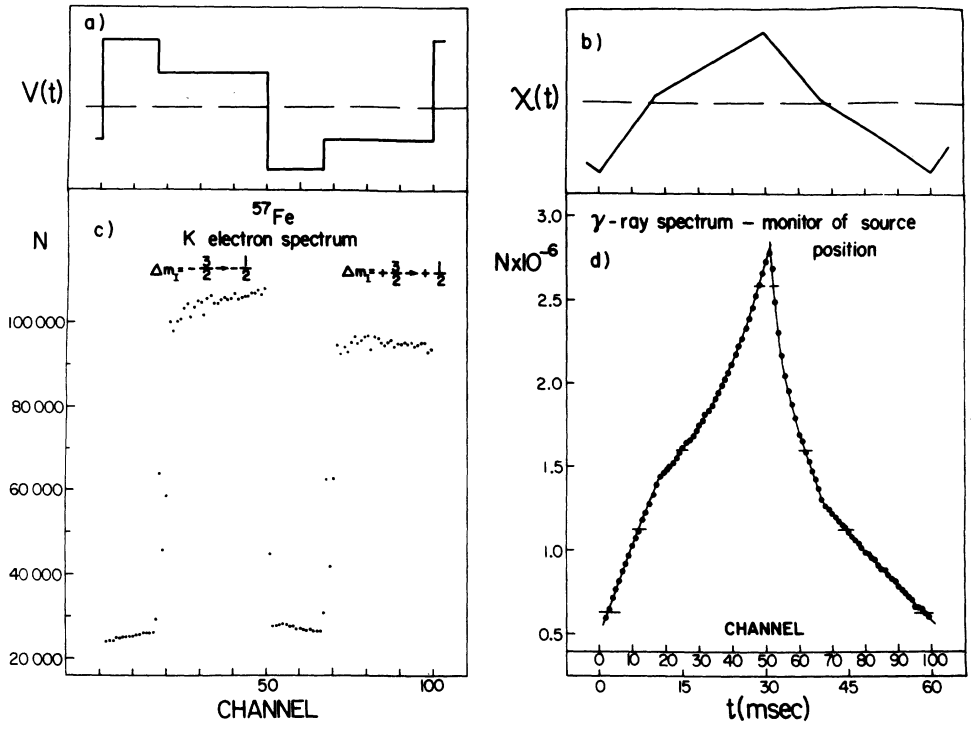

FIG. 8. (a) Reference wave form applied to the source drive, (b) corresponding source displacement, (c) electron spectrum obtained with the electron spectrometer set for detection of K electrons (total measuring time for this run was 89 h), and (d) spectrum of nonresonant radiation scattered from the absorber; channel intervals having the same source position are indicated by horizontal bars.

calculations indicate that the spin polarization of 1s electrons is less than 10^{-5}, the deviation of R_K from unity is a direct measure of the solid angle effect.

Data were collected by alternating the spectrometer field over the K, L_I, and M_I electron lines once a day. To test for the presence of systematic errors due to geometrical factors, measurements were made for two source-absorber separations and at two different periods of the velocity cycle. The signal-to-background ratio $(Y^{\pm}-B^{\pm})/B^{\pm}$ varied considerably as a function of electron energy (Table II). The variations of R_K with source position and frequency as well as the normalized data are shown in Table III.

The data were also corrected for the unresolved 2p electrons (L_{II} and L_{III}) present in the 2s line and 3p, 3d, and 4s ($M_{II} \ldots M_V$ and N_I) electrons in the 3s line. It was assumed that only the 4s electrons in the contaminant contribution might be polarized, and the ratios of internal conversion $L_I/(L_{II}+L_{III}) = 10.7 \pm 0.1$,[18] $M_I/(M_{II}+\ldots+M_V) = 12.08 \pm 0.26$,[19] and $N_I/M_I = 0.0407 \pm 0.0033$[19] measured by Porter[18] and more recently by Fujioka[19] were adopted.

We define a relative spin density

$$\delta_{ns} = \frac{|\psi_{ns}^{\uparrow}(0)|^2}{|\psi_{ns}^{\downarrow}(0)|^2} - 1 .$$

The measured ratios R_L/R_K are related to this spin density δ_{ns} by

$$\frac{R_L}{R_K} = 1 + \frac{\delta_{2s}}{1+[(L_{II}+L_{III})/L_I](2+\delta_{2s})}$$

and

$$\frac{R_M}{R_K} = 1 + \frac{\delta_{3s}}{D} + \frac{\delta_{4s}}{D}\left(\frac{N_I}{M_I}\right)\left(\frac{2+\delta_{3s}}{2+\delta_{4s}}\right),$$

where

TABLE III. Observed counting rate ratios of K, L, and M electrons in iron metal and Fe_2O_3 as a function of frequency and source-absorber distance. The deviation of R_K from unity results from the different solid angles subtended at the absorber by the source for the two corresponding resonant velocities.

		$d=4$ mm $T=60$ msec	$d=2.75$ mm $T=60$ msec	$d=2.75$ mm $T=120$ msec
Fe	R_K	0.9379 ± 0.0021	0.9020 ± 0.0009	0.8815 ± 0.0013
	R_L/R_K	0.9977 ± 0.0031	0.9948 ± 0.0019	0.9926 ± 0.0025
	R_M/R_K		1.0142 ± 0.0079	1.0096 ± 0.0083
Fe_2O_3	R_K		0.9560 ± 0.0011	
	R_L/R_K		0.9947 ± 0.0024	
	R_M/R_K		1.0186 ± 0.0088	

TABLE IV. Measured spin density $\delta_{ns} = |\psi^{\uparrow}_{ns}(0)|^2/|\psi^{\downarrow}_{ns}(0)|^2 - 1$ of s electrons at the nucleus in iron metal and Fe_2O_3 and comparison with theoretical predictions. These data have been corrected for unresolved components as indicated in the text.

		δ_{2s}	δ_{3s}	δ_{4s}
Fe_2O_3	Expt.	-0.0063 ± 0.0024	$+0.0217 \pm 0.0088$	
			$+0.0145 \pm 0.0068$	0
Fe	Expt.	-0.0063 ± 0.0015	or	Ref. 20
			-0.0100 ± 0.0068	$+0.86$
Theory	band theory			
	Ref. 21	-0.0028	$+0.011$	-0.038
	Ref. 22			$+0.026$
	atomic wave fcns.			
	Refs. 7, 23	-0.0051	$+0.021$	$+0.256$

$$D = 1 + \frac{N_I}{M_I}\left(\frac{2+\delta_{3s}}{2+\delta_{4s}}\right)\left(\frac{M_{II}+\cdots+M_V}{M_I}\right)(2+\delta_{3s}).$$

In order to extract the $3s$ spin density from the measurement an estimate must be made of the $4s$ spin density. This quantity was derived by Stearns[20] from systematic measurements of hyperfine fields in the $3d$ series transition metals. She obtained

$$\delta_{4s} = \frac{|\psi^{\uparrow}_{4s}(0)|^2}{|\psi^{\downarrow}_{4s}(0)|^2} - 1 = 0.86 .$$

Table IV shows the final results for the spin density calculated for the two extreme values $\delta_{4s} = 0$ and $\delta_{4s} = 0.86$ for iron metal and $\delta_{4s} = 0$ for Fe_2O_3. The errors quoted are purely statistical and do not include possible systematic errors. These are estimated to be less than 0.03% of the ratios given.

The technique was tested further by studying the decay of the $m_I = \pm\frac{1}{2}$ states for iron metal. The expected polarization effect should be $\frac{1}{3}$ of the effect seen in the decay of the $m_I = \pm\frac{3}{2}$ states. The results of these measurements yielded $\delta_{2s} = (-0.34 \pm 0.15)\%$ and $\delta_{3s} = (+0.44 \pm 0.54)\%$ which agree within the statistical errors with the expected values.

The hyperfine field corresponding to these values of spin polarization can be obtained provided the absolute value of the total ns electron wave function is known. The relationship between the hyperfine field and the net spin density is given by

$$H_{ns} = 4\pi(4.21\times10^4)[\,|\psi^{\uparrow}_{ns}(0)|^2 - |\psi^{\downarrow}_{ns}(0)|^2\,]\,\mathrm{G}$$
$$= 4\pi(4.21\times10^4)\left(\frac{\delta_{ns}}{\delta_{ns}+2}\right)$$
$$\times[\,|\psi^{\uparrow}_{ns}(0)|^2 + |\psi^{\downarrow}_{ns}(0)|^2\,]\,\mathrm{G}.$$

All calculations of densities of *core* electrons based either on band theory[21] or on atomic models[7] agree within a few percent. Thus hyperfine fields can be extracted from the present data with no ambiguity other than that of the determination of the hyperfine field contributed by the $4s$ electrons. Hyperfine fields obtained by combining the present measurements with the density calculations of Bagus and Liu[7] are displayed in Table V.

VI. DISCUSSION

This experiment yields a *direct* measurement of the ratios of spin-up to spin-down densities of s electrons in individual s subshells and an *indirect* measurement of the contact hyperfine fields at the nuclear site contributed by the net spin density of each s subshell. Whereas there is no experimental ambiguity as to the measurements of the $2s$ electronic densities, conclusions on the $3s$ contributions in iron metal cannot be drawn from the present data without an independent determination of the polarization of the $4s$ conduction electrons. However, as can be seen in Table V, the total field contributed by the $2s$, $3s$, and $4s$ electrons is not very sensitive to the value adopted for the $4s$ polarization. The expected contribution from the $1s$ electrons is of the order of -10 to -50 kG.[6] The very large negative value obtained for $H_{2s}+H_{3s}+H_{4s}$ must be compared with the accepted value $H_{\mathrm{total}} = -339$ kG for iron metal. The discrepancy between this figure and the field estimated from the present experiment indicates that there must exist either strong positive contributions from interactions other than the Fermi contact term, or undetected systematic errors in the present data. A

TABLE V. Individual shell contributions to the hyperfine field at the nucleus calculated from the measured spin polarization and the corresponding charge densities calculated by Bagus and Liu (Ref. 7). The 600-kG hyperfine field contributed by the $4s$ electrons was taken from the measurements of Stearns (Ref. 20).

	H_{2s}	H_{3s}	H_{4s}	$H_{2s}+H_{3s}+H_{4s}$
		$+517 \pm 242$	0	-1127 ± 460
Fe	-1644 ± 391		or	
		-357 ± 243	+600	-1401 ± 460
Fe_2O_3	-1644 ± 626	$+770 \pm 312$		-874 ± 700

new spectrometer with an order of magnitude increase in transmission and a factor of 3 or 4 improvement in energy resolution is being built. The ability to collect data with high statistical accuracy and better resolution over a much shorter time interval will reduce systematic errors and will, in addition, allow for thorough checks of such errors.

In the case of Fe_2O_3, there are no 4s electron contributions and $H_{2s}+H_{3s}$ was thus obtained directly. The result agrees with the total field obtained from Mössbauer spectra, $H_{\text{total}} = -515$ kG. It must be noted that the large errors in H arise from the addition of errors in separate contributions. The net polarization of individual s shell electrons is the appropriate quantity to extract from this type of data. The following conclusions can be drawn:

(a) The data support the theoretically predicted sign and order of magnitude of the spin polarization of the 2s electrons in Fe and Fe_2O_3.

(b) The 3s electron polarization in iron may either be large and positive and consistent with the Wakoh and Yamashita[21] prediction of small 4s polarization *or* be small and negative in agreement with the large positive 4s polarization measured by Stearns[20] and supported by recent calculations by Duff.[24]

It should, however, be stressed that the results presented in Table IV, while not unambiguous, were obtained under widely different experimental conditions such as source-absorber distance, period of motion, Mössbauer resonance velocity, sign of isomer shift, and degree of polarization of absorber. The consistency of the results in indeed encouraging and warrants further efforts to improve the precision of s electron spin density measurements performed by this particular technique.

ACKNOWLEDGMENTS

We would like to thank Professor G. M. Rothberg for his substantial contributions to this work during the planning stages and early experimental phases, and Dr. M. B. Stearns and Dr. T. P. Das for many stimulating discussions on the interpretation of the results and their correlation to other data. We are particularly grateful to Professor A. Freeman for his enthusiasm, advice, and encouragement over the years.

---

†Work supported by the National Science Foundation.

*Present address: Department of Physics, Purdue University, Lafayette, Indiana 47907.

‡Present address: Department of Physical Chemistry, Katholieke Universiteit, Nijmegen, Netherlands.

[1]C. J. Song, J. Trooster, N. Benczer-Koller, and G. M. Rothberg, Phys. Rev. Lett. 29, 1165 (1972).

[2]E. Fermi, Z. Phys. 60, 320 (1930); E. Fermi and E. Segrè, Z. Phys. 82, 729 (1933).

[3]A. Abragam and M. H. L. Pryce, Proc. R. Soc. A205, 135 (1951).

[4]R. M. Sternheimer, Phys. Rev. 86, 316 (1952).

[5]S. S. Hanna, J. Heberle, G. J. Perlow, R. S. Preston and D. H. Vincent, Phys. Rev. Lett. 4, 513 (1960).

[6]R. E. Watson and A. J. Freeman, Phys. Rev. 123, 2027 (1961); A. J. Freeman and R. E. Watson, in *Magnetism*, edited by G. T. Rado and H. Suhl (Academic, New York, 1965), Vol. II; R. E. Watson and A. J. Freeman, *Hyperfine Interaction*, edited by A. J. Freeman and R. Frankel (Academic, New York, 1967).

[7]P. S. Bagus and B. Liu, Phys. Rev. 148, 79 (1966).

[8]H. U. Freund and J. C. McGeorge, Z. Phys. 238, 6 (1970).

[9]M. E. Rose, *Internal Conversion Processes*, edited by J. H. Hamilton (Academic, New York, 1966); E. L. Church and J. Weneser, Ann. Rev. Nucl. Sci. 10, 193 (1960).

[10]M. E. Rose, L. C. Biedenharn, and G. B. Arfken, Phys. Rev. 85, 5 (1952).

[11]I. M. Band, L. A. Sliv, and M. B. Trzhaskovskaya, Nucl. Phys. A 156, 170 (1970).

[12]E. M. Anderson, M. A. Listengarten, and M. A. Khanonkind, Izv. Akad. Nauk. SSSR Ser. Fiz. 34, 850 (1970).

[13]M. Fujioka, U. S.-Japan Seminar on Hyperfine Interactions Involving Excited Nuclei, August 30–Sept. 1, 1972, Kobe, Japan (unpublished).

[14]P. S. Bagus, A. J. Freeman, and F. Sasaki, Phys. Rev. Lett. 30, 850 (1973).

[15]C. S. Fadley, D. A. Shirley, A. J. Freeman, P. S. Bagus, and J. V. Mallow, Phys. Rev. Lett. 23, 1397 (1969).

[16]C. M. Witcher, Phys. Rev. 60, 32 (1941).

[17]E. Kankeleit, Rev. Sci. Instr. 35, 194 (1964).

[18]F. T. Porter and M. S. Freedman, Phys. Rev. C 3, 2285 (1971).

[19]T. Shinohara and M. Fujioka, Phys. Rev. B 7, 37 (1973).

[20]M. B. Stearns, Phys. Rev. B 4, 4081 (1971); International Symposium on Perspectives for Hyperfine Interactions in Magnetically Ordered Systems by N.M.R. and Other Methods, L'Aquila, Italy, Sept. 11–15, 1972 (unpublished); and private communications.

[21]S. Wakoh and J. Yamashita, J. Phys. Soc. Jap. 25, 1272 (1968).

[22]K. S. Duff and T. P. Das, Phys. Rev. B 3, 2294 (1971).

[23]M. Morita, K. Sugimoto, M. Yamada, and Y. Yokoo, Prog. Theor. Phys. 41, 996 (1969).

[24]T. P. Das (private communication).